

Pauli Decomposition over Commuting Subsets: Applications in Gate Synthesis, State Preparation, and Quantum Simulations

Swathi S. Hegde¹, K. R. Koteswara Rao² and T. S. Mahesh^{1*}

¹*Department of Physics and NMR Research Center,*

Indian Institute of Science Education and Research, Pune 411008, India

²*Fakultät Physik, Technische Universität Dortmund, D-44221 Dortmund, Germany*

A key task in quantum computation is the application of a sequence of gates implementing a specific unitary operation. However, the decomposition of an arbitrary unitary operation into simpler quantum gates is a nontrivial problem. Here we propose a general and robust protocol to decompose any target unitary into a sequence of Pauli rotations. The procedure involves identifying a commuting subset of Pauli operators having a high trace overlap with the target unitary, followed by a numerical optimization of their corresponding rotation angles. The protocol is demonstrated by decomposing several standard quantum operations. The applications of the protocol for quantum state preparation and quantum simulations are also described. Finally, we describe an NMR experiment implementing a three-body quantum simulation, wherein the above decomposition technique is used for the efficient realization of propagators.

I. INTRODUCTION

Quantum devices have the capability to perform several tasks with efficiencies beyond the reach of their classical counterparts [1, 2]. An important criterion for the physical realization of such devices is to achieve precise control over the quantum dynamics [3]. The circuit model of quantum computation is based on the realization of a desired unitary in terms of simpler quantum gates. However, arbitrarily precise decomposition of a general unitary U_T in the form

$$U_T = U_m \cdots U_2 U_1, \quad (1)$$

is a nontrivial task. Here each of the U_j 's is either of lower complexity or acts on smaller subsystems. Such a decomposition is said to be efficient if (i) m scales polynomially with the system size n and (ii) spatial and temporal overhead of each U_j scales polynomially with n .

The decomposition of a unitary operator corresponding to a Hamiltonian $\mathcal{H} = \mathcal{H}_A + \mathcal{H}_B$, where $[\mathcal{H}_A, \mathcal{H}_B] = 0$, is trivial, i.e., $U_T = e^{-i\mathcal{H}t} = e^{-i\mathcal{H}_A t} e^{-i\mathcal{H}_B t}$. When $[\mathcal{H}_A, \mathcal{H}_B] \neq 0$, one can discretize the time, $\delta = t/m$, and use the Trotter's formula [4]

$$U_T = [e^{-i\mathcal{H}_A \delta} e^{-i\mathcal{H}_B \delta}]^m + \mathcal{O}(\delta^2) \quad (2)$$

or its symmetrized form [5]

$$U_T = \left[e^{-i\mathcal{H}_A \delta/2} e^{-i\mathcal{H}_B \delta} e^{-i\mathcal{H}_A \delta/2} \right]^m + \mathcal{O}(\delta^3). \quad (3)$$

For a time-dependent Hamiltonian $\mathcal{H}(t)$, one needs to use Dyson's time ordering operator or the Magnus expansion, and then decompose the time discretized components [6]. However, for a given unitary U_T , such a decomposition

may not be obvious or even after the decomposition, the individual pieces themselves may involve matrix exponentials of non-commuting operators thus failing to reduce the complexity.

Several advanced decomposition routines have been suggested for arbitrary unitary decomposition. Barenco *et al.* have shown that XOR gates along with local gates are universal, and in terms of these elementary gates they have explicitly decomposed several standard quantum operations [7]. Tucci presented an algorithm to decompose an arbitrary unitary into single and two-qubit gates using a mathematical technique called CS decomposition [8]. Khaneja *et al.* used Cartan decomposition of the semi-simple lie group $SU(2^n)$ for the unitary decomposition [9]. A method to realize any multiqubit gate using fully controlled single-qubit gates using Grey code was given by Vartiainen *et al.* [10]. Möttönen *et al.* have presented a cosine-sine matrix decomposition method synthesizing the gate sequence to implement a general n -qubit quantum gate [11]. Recently, Ajoy *et al.* also developed an ingenious algorithm to decompose an arbitrary unitary operator using algebraic methods [12]. More recently, this method was utilized in the experimental implementation of mirror inversion and other quantum state transfer protocols [13]. Manu *et al.* have shown several unitary decompositions by case-by-case numerical optimizations [14].

In this article, we propose a general algorithm to decompose an arbitrary unitary upto a desired precision. It is distinct from the above approaches in several ways. Firstly, our method considers generalized rotations of commuting Pauli operators which are more amenable for practical implementations via optimal control techniques. Secondly, being a numerical procedure, it considers various experimentally relevant parameters such as robustness with respect to fluctuations in the control parameters, minimum rotation angles etc. Besides, the procedure can be extended for quantum circuits, quantum simulations, quantum state preparations, and prob-

*Electronic address: mahesh.ts@iiserpune.ac.in

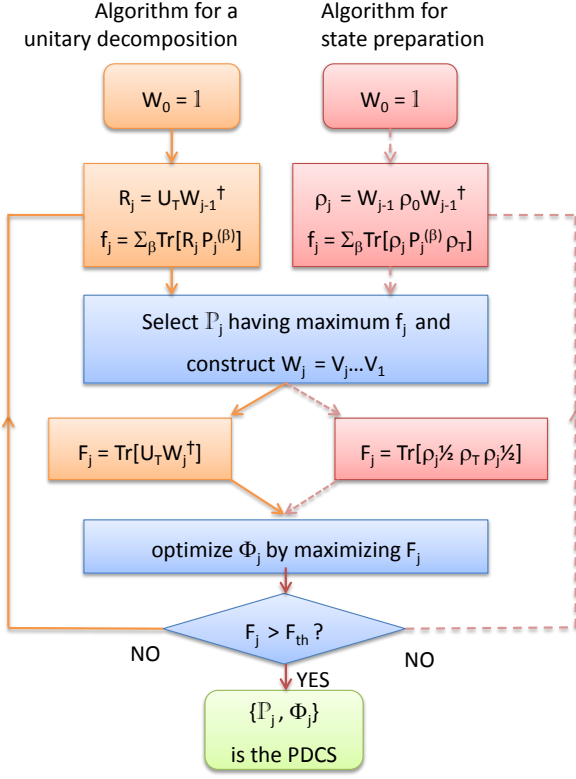


FIG. 1: (Color online) The flowchart describing PDCS algorithm for unitary decomposition (left) and state preparation (right, dashed).

ably in some cases even for nonunitary synthesis.

The paper is organized as follows: A detailed explanation of the algorithm for arbitrary unitary decomposition is presented in section II. Section III deals with the applications of the algorithm with explicit demonstrations involving the decomposition of standard gate-synthesis, quantum circuit designs, certain quantum state preparations, and for quantum simulations. Finally we conclude in section IV.

II. ALGORITHM

In the following, we describe an algorithm for Pauli decomposition over commuting subsets (PDCS) for arbitrary unitary operators. Although for the sake of simplicity we utilize 2-level quantum systems, the protocol applies equally well to any d -level quantum systems.

Let U_T be the desired unitary operator of dimension $N = 2^n$ to be applied on an n -qubit system. We seek an m -rotor decomposition $W_m = V_m V_{m-1} \dots V_1 \approx U_T$, where the decomposed unitaries V_j with $j \in [1, m]$ have the form

$$V_j = e^{-i \sum_\beta P_j^{(\beta)} \phi_j^{(\beta)}}. \quad (4)$$

Here $\{P_j^{(\beta)}\} \equiv \mathbb{P}_j$ is a maximally commuting subset of n -qubit Pauli operators, $\{\phi_j^{(\beta)}\} \equiv \Phi_j$ is the set of corresponding rotation angles, and the index β runs over the elements of \mathbb{P}_j . In general, for an n -qubit case, a maximal commuting subset \mathbb{P}_j can have at most $N - 1$ elements. The fidelity F_m of the decomposition, defined by

$$F_m = \langle U_T | W_m \rangle = |\text{Tr}[U_T^\dagger W_m] / N|, \quad (5)$$

should be larger than a desired threshold F_{th} .

The flowchart for the PDCS algorithm is shown in Fig. 1. We now describe an algorithm to build W_m in m steps. To begin with, we start with $W_0 = \mathbb{1}$. The j th step of the algorithm consists of the following processes:

1. Calculate the residual propagator $R_j = U_T W_{j-1}^\dagger$.
2. Selection of the commuting subset \mathbb{P}_j having the maximum overlap $f_j = \sum_\beta \text{Tr}[R_j P_j^{(\beta)}]$ with the residual unitary R_j .
3. Setting up the decomposition W_j and numerically optimizing the rotation angles $\{\Phi_1, \dots, \Phi_j\}$ by maximizing the fidelity $F_j = \langle W_j | U_T \rangle$, where $W_j = V_j \dots V_1$.

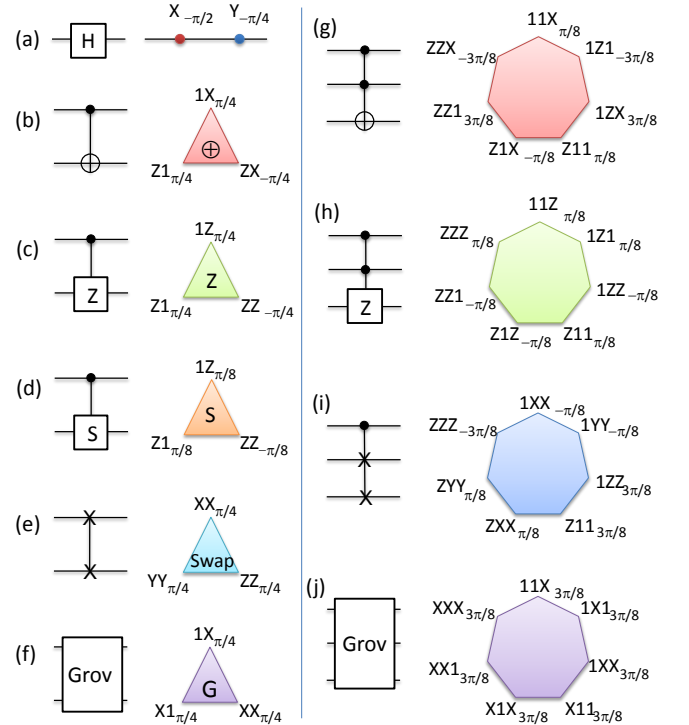


FIG. 2: (Color online) PDCS of some standard quantum gates: (a) single-qubit Hadamard, (b) c-NOT, (c) c-Z, (d) c-S, (e) SWAP, (f) 2-qubit Grover iterate, (g) Toffoli, (h) c^2 -Z, (i) Fredkin, and (j) 3-qubit Grover iterate. The individual rotors are represented by dots, triangles, and heptagons depending on number of Pauli operators (indicated at the vertices) in each rotor. The corresponding rotation angles are indicated by subscripts.

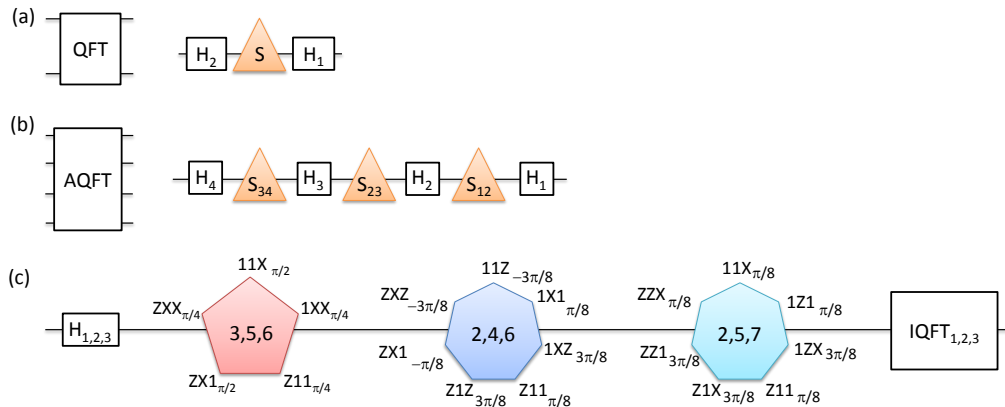


FIG. 3: (Color online) PDCS of (a) 2-qubit Quantum Fourier Transform (QFT), (b) 4-qubit approximate QFT (AQFT), and (c) 7-qubit Shor's circuit for factorizing 15. In (b), each S gate acts on a pair of qubits as indicated by the subscripts.

These steps can be iterated upto m -steps until the fidelity $F_m > F_{\text{th}}$ of a desired value is reached.

In general, the solutions to the decomposition may not be unique. However, it is desirable to attain a decomposition that is most suitable for experimental implementations. In this regard, we look for solutions with minimum rotation angles $\{\Phi_j\}$, which can be obtained by using a suitable penalty function in step 3 of the above algorithm.

III. APPLICATIONS

A. PDCS of quantum gates and circuits

In this section we illustrate PDCS of several standard quantum gates. As described in Eq. 4, the j th decomposition is expressed in terms of the commuting Pauli operators \mathbb{P}_j and the corresponding rotation angles Φ_j . Further, a specific operator $P_j^{(\beta)} \in \mathbb{P}_j$ can be expressed as a tensor product of single-qubit Pauli operators X , Y , Z , and the identity matrix $\mathbb{1}$.

Exact PDCS of several standard quantum gates are shown in Fig. 2. For a single-qubit Hadamard operation (Fig. 2(a)), we obtain a decomposition with two noncommuting rotations, as is well known [1]. Here $\mathbb{P}_1 = X$, $\mathbb{P}_2 = Y$ and the corresponding rotation angles $\Phi_1 = -\pi/2$, $\Phi_2 = -\pi/4$, are indicated by the subscripts.

In the two-qubit case, the maximal commuting subset can have only three Pauli operators and there are only 15 such subsets. Figs. 2(b-e) describe decompositions of several two-qubit gates namely c-NOT, c-Z, c-S, and SWAP gate. Here $Z = \begin{bmatrix} 1 & 0 \\ 0 & -1 \end{bmatrix}$ and $S = \begin{bmatrix} 1 & 0 \\ 0 & i \end{bmatrix}$. It is interesting to note that each of these gates needs a single subset of commuting Pauli operators. Such a rotation can be obtained by a single matrix exponential and can be thought of as a single generalized rotation in the Pauli space. We refer to such a generalized rotation as a rotor, and since it consists of three operators, we represent it

by a triangle. In practice, the individual components of a single rotor can be implemented either simultaneously, or in any order. We find that even a 2-qubit Grover iterate, i.e., $G = 2|\psi\rangle\langle\psi| - \mathbb{1}$, where $|\psi\rangle = (|00\rangle + |01\rangle + |10\rangle + |11\rangle)/2$, can be realized as a single rotor (Fig. 2(f)).

For three-qubits, the maximal commuting subset can have only seven commuting Pauli operators and there are 135 distinct subsets. Figs. 2(g-j) describe Toffoli, c^2 -Z, Fredkin, and 3-qubit Grover iteration respectively. Again we find that a single heptagon rotor suffices for realizing each of the standard gates. Similarly, in the case of four-qubits, a maximal commuting subset can have 15 operators and one can verify that a basic gate such as c^3 -NOT, c^3 -Z, etc. can be realized by a single rotor.

It is always possible to decompose a multi-qubit quantum circuit in terms of single- and two-qubit gates [7]. As examples, we shall consider PDCS of a few quantum circuits (Fig. 3). The two-qubit Quantum Fourier Transform (QFT) circuit can be exactly decomposed into three rotors as shown in Fig. 3(a). As another example, PDCS of the 4-qubit approximate QFT (AQFT) circuit [15] results in only single-qubit and two-qubit rotors as shown in Fig. 3(b). Similarly, PDCS of the 7-qubit Shor's circuit for factoring the number 15 involves at most three-qubit rotors as shown in Fig. 3(c) [16]. In this sense, PDCS of multiqubit quantum gates and quantum circuits is scalable with increasing system size.

B. Quantum state preparation

Here the goal is to prepare a target state ρ_T starting from a given initial state ρ_0 . In general the unitary operator, connecting the initial and target states, itself is not unique. The procedure is similar to that described in the previous section, and is summarized in the flowchart shown in Fig. 1. Here the selection of commuting Pauli operators \mathbb{P}_j is based on the overlap $f_j = \sum_{\beta} \text{Tr}[\rho_j P_j^{(\beta)} \rho_T]$, where $\rho_j = W_j \rho_0 W_j^\dagger$ is the intermediate state after j th decomposition. As explained

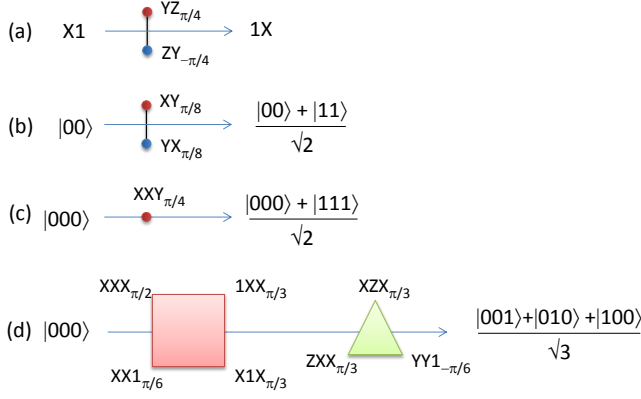


FIG. 4: (Color online) PDCS of some state to state transfers: (a) polarization transfer (INEPT) and (b-d) preparation of Bell, GHZ, and W states respectively starting from pure states.

before, we select the commuting subset \mathbb{P}_j having the maximum overlap f_j and optimize the phases Φ_j by maximizing the Uhlmann fidelity

$$F_j = \langle \rho_j | \rho_T \rangle = \text{Tr}[\rho_j^{1/2} \rho_T \rho_j^{1/2}]. \quad (6)$$

Again, m iterations are carried out until $F_m \geq F_{\text{th}}$ is realized.

Fig. 4 displays PDCS of some standard state to state transfers. The polarization transfer in a pair of qubits (popularly known as INEPT [17]) requires a single rotor having a pair of bilinear operators (Fig. 4(a)). The preparation of a Bell and GHZ states respectively from $|00\rangle$ and $|000\rangle$ states also require a single rotor (Fig. 4(b-c)). However, the preparation of a three-qubit W-state is somewhat more elaborated, and requires two rotors (Fig. 4(d)). Although these decompositions are not unique, it is possible to optimize them based on the experimental conditions. Here one can notice that although a maximal commuting subset can have up to $N - 1$ elements, it is often possible to decompose a multi-qubit operation over a smaller commuting subset.

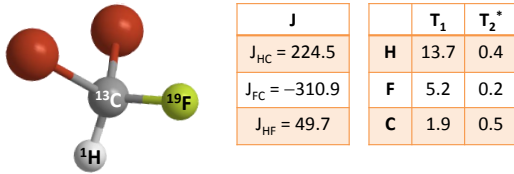


FIG. 5: (Color online) Dibromofluoromethane consisting of three nuclear spin qubits ^1H , ^{13}C and ^{19}F . The tables display the values of indirect spin-spin coupling constants (J) in Hz, and the relaxation time constants (T_1 , and T_2^*) in seconds.

C. Quantum simulation

Utilizing controllable quantum systems to mimic the dynamics of other quantum systems is the essence of quantum simulation [18]. Various quantum devices have already demonstrated quantum simulations of a number of quantum mechanical phenomena (for example, [19–22]). An important application of the decomposition technique described above is in the experimental realization of quantum simulations. To illustrate this fact, we experimentally carry out quantum simulation of a three-body interaction Hamiltonian using a three-qubit system. While such a Hamiltonian is physically unnatural, simulating such interactions has interesting applications such as in quantum state transfer [23]. Specifically, we simulate the dynamics under the Hamiltonian

$$\mathcal{H}_S = X11 + 1X1 + 11X + J_{123}ZZZ, \quad (7)$$

where J_{123} is the three-body interaction strength. A slightly different three-body Hamiltonian simulated earlier by Cory and coworkers [24] consisted of only the last term. The presence of other terms which are noncommuting with the 3-body term necessitates an efficient decomposition of the overall unitary.

We use three spin-1/2 nuclei of dibromofluoromethane (Fig. 5) dissolved in acetone- D_6 as our three-qubit system. All the experiments are carried out on a 500 MHz Bruker NMR spectrometer at an ambient temperature of 300 K. In the triply rotating frame at resonant offsets, the internal Hamiltonian of the system is given by

$$\mathcal{H}_{\text{int}} = [J_{\text{HF}}ZZ1 + J_{\text{HC}}Z1Z + J_{\text{FC}}1ZZ] \pi/2, \quad (8)$$

and the values of the indirect coupling constants $\{J_{\text{HF}}, J_{\text{HC}}, J_{\text{FC}}\}$ are as in Fig. 5. This internal Hamiltonian along with the external control Hamiltonians provided by the RF pulses are used in the following to mimic the three-body Hamiltonian in Eqn. 7.

The traceless part of the thermal equilibrium state of the 3-qubit NMR spin system is given by $\rho_{\text{eq}} = (Z11 + 1Z1 + 11Z)/2$ [17]. The initial state $\rho(0) = (X11 + 1X1 + 11X)/2$ is prepared by applying a 90° RF-pulse about Y . The goal is to subject the three-spin system to an effective three-body Hamiltonian \mathcal{H}_S and monitor the evolution of its state $\rho(t) = U_S(t)\rho(0)U_S(t)^\dagger$, where $U_S(t) = e^{-i\mathcal{H}_S t}$. We choose to experimentally observe

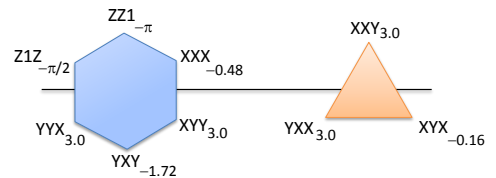


FIG. 6: (Color online) PDCS of $U_S(\tau) = \exp(-i\mathcal{H}_S \tau)$ for $J_{123} = 5$ Hz and $\tau = 0.8$ s.

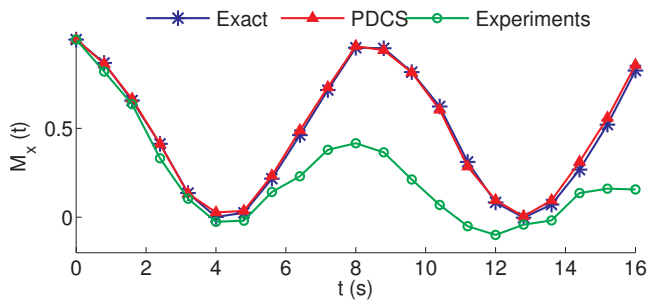


FIG. 7: (Color online) Magnetization vs time.

the transverse magnetization

$$M_x(k\tau) = \text{Tr}[\rho(k\tau)(X\mathbb{1}\mathbb{1} + \mathbb{1}X\mathbb{1} + \mathbb{1}\mathbb{1}X)/2] \quad (9)$$

for $J_{123} = 5$ Hz at discrete time intervals $k\tau$, where $k = \{0, \dots, 20\}$ and $\tau = 0.8$ s.

The PDCS of U_S shown in Fig. 6 consists of two rotors: a hexagon followed by a triangle. We utilized bang-bang (BB) control technique for generating each of the two rotors [25]. The duration of each BB-sequence was about 7 ms and fidelities were above 0.98 averaged over a 10% inhomogeneous distribution of RF amplitudes. The results of the experiments (hollow circles) and their comparison with numerical simulation of the PDCS (triangles) and exact numerical values (stars) are shown in Fig. 7. The first experimental data point was obtained after a simple 90 degree RF pulse and was normalized to 1. The k^{th} point is obtained by k iterations of the BB-sequence for $U_S(\tau)$. While the experimental curve displays the same period and phase as that of the simulated curve, the steady decay in amplitude is mainly due to decoherence and other experimental imperfections such as RF inhomogeneity and nonlinearities of the RF channel.

To compare the efficiency of PDCS with that of Trotter decomposition (in Eq. 2 and 3), we calculate the fidelities (F) of the decomposed propagator with the exact propagator $U_S(\tau)$ as a function of number m of rotors (see Fig. 8). It can be observed that, with increasing number of rotors, PDCS fidelity converges faster than the Trotter.

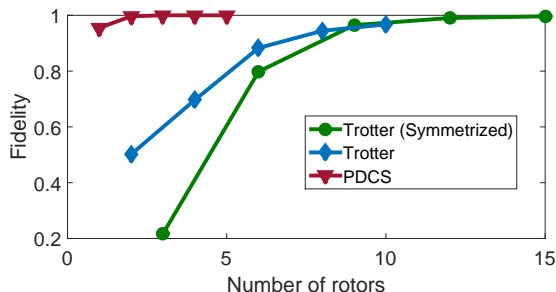


FIG. 8: (Color online) Fidelity (F_m) vs number (m) of rotors in the decompositions.

IV. CONCLUSIONS

In this work we proposed a generalized numerical algorithm based on Pauli decomposition over commuting subsets (PDCS). The aim of the algorithm is to decompose an arbitrary target unitary into simpler unitaries, referred to as rotors. Each rotor consists of only commuting subset of Pauli operators. These rotors are optimized to be robust against experimental errors by minimizing the rotation angles and by considering other control errors. Thus apart from providing an intuitive and topological representation of an arbitrary quantum circuit, the method is also useful for its efficient physical realization.

We demonstrated the robustness and efficiency of the decomposition using numerous examples of quantum gates and circuits. It is interesting to note that several standard quantum gates correspond to single rotors. We also discussed the applications of PDCS in quantum state-to-state transfers and illustrated it using several examples.

Another important application of PDCS is in quantum simulations. As an example, we described the quantum simulation of a three-body interaction. We used PDCS algorithm to decompose the unitary corresponding to such a Hamiltonian and found it to be more efficient than Trotter decomposition in terms of the number of rotors. Further, we have demonstrated the quantum simulation by experimentally monitoring the evolution of magnetization using a three qubit NMR system. The experimental results matched with the numerical simulations upto a decay factor arising predominantly due to decoherence.

We believe such unitary decomposition strategies combined with sophisticated optimal control techniques will greatly assist in efficient quantum control.

Acknowledgments

We thank Prof. Anil Kumar, IISc, Bangalore for providing us the three-qubit NMR register. We also acknowledge useful discussions with Sudheer Kumar. This work was partly supported by DST Project No. DST/SJF/PSA-03/2012-13.

-
- [1] M. A. Nielsen and I. L. Chuang, *Quantum computation and quantum information* (Cambridge university press, 2010).
- [2] J. Preskill, California Institute of Technology (1998).
- [3] D. P. DiVincenzo, *Fortschritte der Physik* **48**, 771 (2000).
- [4] H. F. Trotter, *Proceedings of the American Mathematical Society* **10**, 545 (1959).
- [5] A. Sornborger and E. Stewart, *Physical Review A* **60**, 1956 (1999).
- [6] J. J. Sakurai and J. Napolitano, *Modern quantum mechanics* (Addison-Wesley, 2011).
- [7] A. Barenco, C. H. Bennett, R. Cleve, D. P. DiVincenzo, N. Margolus, P. Shor, T. Sleator, J. A. Smolin, and H. Weinfurter, *Physical Review A* **52**, 3457 (1995).
- [8] R. R. Tucci, arXiv preprint quant-ph/9902062 (1999).
- [9] N. Khaneja and S. J. Glaser, *Chemical Physics* **267**, 11 (2001).
- [10] J. J. Vartiainen, M. Möttönen, and M. M. Salomaa, *Physical review letters* **92**, 177902 (2004).
- [11] M. Möttönen, J. J. Vartiainen, V. Bergholm, and M. M. Salomaa, *Phys. Rev. Lett.* **93**, 130502 (2004).
- [12] A. Ajoy, R. K. Rao, A. Kumar, and P. Rungta, *Physical Review A* **85**, 030303 (2012).
- [13] K. Rao, T. Mahesh, and A. Kumar, arXiv preprint arXiv:1307.5220 (2013).
- [14] V. Manu and A. Kumar, *Physical Review A* **89**, 052331 (2014).
- [15] A. Barenco, A. Ekert, K.-A. Suominen, and P. Törmä, *Physical Review A* **54**, 139 (1996).
- [16] L. M. Vandersypen, M. Steffen, G. Breyta, C. S. Yannoni, M. H. Sherwood, and I. L. Chuang, *Nature* **414**, 883 (2001).
- [17] J. Cavanagh, W. J. Fairbrother, A. G. Palmer III, and N. J. Skelton, *Protein NMR spectroscopy: principles and practice* (Academic Press, 1995).
- [18] R. Feynman, *International Journal of Theoretical Physics* **21**, 467 (1982).
- [19] X. Peng, J. Du, and D. Suter, *Physical Review A* **71**, 012307 (2005).
- [20] D. I. Tsomokos, S. Ashhab, and F. Nori, *Physical Review A* **82**, 052311 (2010).
- [21] M. Greiner, O. Mandel, T. Esslinger, T. W. Hänsch, and I. Bloch, *nature* **415**, 39 (2002).
- [22] S. S. Hegde, H. Katiyar, T. Mahesh, and A. Das, *Physical Review B* **90**, 174407 (2014).
- [23] J. Zhang, X. Peng, and D. Suter, *Physical Review A* **73**, 062325 (2006).
- [24] C. Tseng, S. Somaroo, Y. Sharf, E. Knill, R. Laflamme, T. F. Havel, and D. G. Cory, *Physical Review A* **61**, 012302 (1999).
- [25] G. Bhole, T. Mahesh, *et al.*, arXiv preprint arXiv:1512.08385 (2015).